EUROPHYSICS LETTERS 15 February 2005

Europhys. Lett., **69** (4), pp. 602–608 (2005)
DOI: 10.1209/epl/i2004-10398-7

Resistance fluctuations near integer quantum Hall transitions in mesoscopic samples

C. Zhou[1](*) and M. Berciu[2]

[1] *Department of Electrical Engineering, Princeton University Princeton, NJ 08544, USA*
[2] *Department of Physics and Astronomy, University of British Columbia Vancouver, BC V6T 1Z1, Canada*

received 18 November 2004; accepted in final form 20 December 2004
published online 14 January 2005

PACS. 73.23.-b – Electronic transport in mesoscopic systems.
PACS. 73.43.-f – Quantum Hall effects.
PACS. 71.30.+h – Metal-insulator transitions and other electronic transitions.

Abstract. – We perform first-principles simulations to study the resistance fluctuations of mesoscopic samples, near transitions between quantum Hall plateaus. We use six-terminal geometry and sample sizes similar to those of real devices and calculate the Hall and longitudinal resistances using the Landauer formula. Our simulations recapture all the observed experimental features. We then use a generalization of the Landauer-Büttiker model, based on the interplay between tunneling and chiral currents, to explain the three regimes with distinct fluctuations observed, and identify the central regime as the critical region.

Although the Integer Quantum Hall Effect (IQHE) is generally well understood, recent experiments on mesoscopic samples [1–3] uncovered unexpected behavior in the seemingly noisy fluctuations of the Hall (R_H) and longitudinal (R_L) resistances. Previously, resistance fluctuations were observed in mesoscopic samples with a phase coherence length larger than the sample size [4–7]; they are totally random, similar to universal conductance fluctuations [8]. In contrast, Peled *et al.* find [1,2] that the transition between the n-th and $(n+1)$-th IQHE plateaus has three distinct regimes: i) on the high-B side, both R_H and R_L have large but *correlated* fluctuations, such that $R_L + R_H = h/ne^2$; ii) for intermediate B values, R_H and R_L exhibit *uncorrelated* fluctuations; and iii) on the low-B side, $R_H = h/(n+1)e^2$ is quantized while R_L fluctuates. For $n = 0$, regions i) and ii) are replaced by the transition to the insulating phase [1]. Moreover, $R_L + R_H = R_{2t}$ holds at all B values [2] (the two-terminal resistance R_{2t} is defined below). Changing the sign of the magnetic field $B \to -B$ also has interesting consequences [3], which we discuss later. In this letter, we explain the physics behind these observations in a unified theory.

The relation $R_L + R_H = R_{2t}$ was first proposed by Streda *et al.* [9], while the fluctuations of regime iii) are reminiscent of Jain and Kivelson's theory on the resistance fluctuations of

(*) Current address: Oak Ridge National Laboratory - PO Box 2008 MS 6164, Oak Ridge, TN 37831-6164, USA.

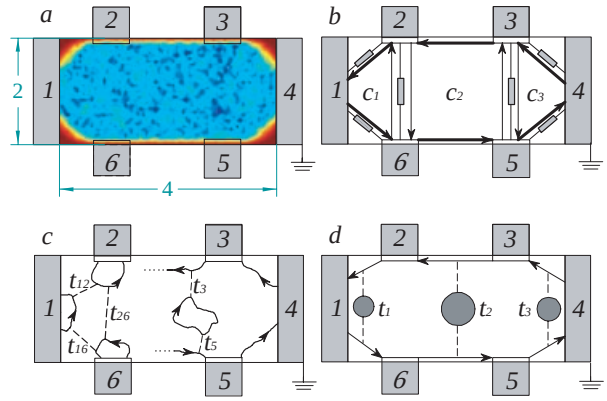

Fig. 1 – (Color online) (a) Typical potential $V_d + V_b$ of a $4\,\mu\text{m} \times 2\,\mu\text{m}$ sample. (b) Chiral (arrows) and tunneling (resistors) currents in our model. This direction of chiral currents corresponds to B entering the page. (c) Some semi-classical current distributions parameterized by our model. (d) Jain-Kivelson tunneling for high ν. See text for further details.

narrow samples [10]. These results were questioned by Büttiker [11], based on formulas derived for a four-terminal geometry [12,13]. We take an approach similar to Büttiker's and use the multi-probe Landauer formula [12–14] to calculate the resistances. However, we mirror the experiments by including all six terminals in our model, *i.e.* the four voltage probes plus the source and the drain for the electrical current. The six-terminal geometry is necessary to compute both R_H and R_L and is one of the main differences between this work and other theoretical investigations of "conductance fluctuations" in two- or four-terminal geometries (*e.g.*, see [15]). Our model enables us to reveal the very rich physics of the mesoscopic IQHE.

The response function of the six-terminal mesoscopic Hall bar is a 6×6 conductance matrix $\hat{g}$, with which the current-voltage relation reads $I_\alpha = \sum_\beta g_{\alpha\beta} V_\beta$. Here, I_α is the out-going current on lead $\alpha = 1, \cdots, 6$ and V_α is the leads's voltage. $\hat{g}$ is calculated [14] by solving a multi-channel scattering problem: $g_{\alpha,\beta\neq\alpha} = (e^2/h) \sum_{i,j} |t_{\alpha i,\beta j}|^2 = (e^2/h) p_{\beta\to\alpha}$, where $t_{\alpha i,\beta j}$ is the transmission amplitude from the j-th transverse channel of lead β into the i-th transverse channel of lead α for an electron at the Fermi energy E_F; $p_{\beta\to\alpha}$ is then the total probability to scatter from contact β into α. Charge conservation and gauge invariance require that $\sum_\alpha g_{\alpha\beta} = \sum_\beta g_{\alpha\beta} = 0$. Diagonal elements then must be given by $g_{\alpha\alpha} = -\sum_{\beta\neq\alpha} g_{\alpha\beta} = -\sum_{\beta\neq\alpha} g_{\beta\alpha}$. This imposes a constraint on the off-diagonal elements of $\hat{g}$ for each value of α.

Our model is sketched in fig. 1(a). Six perfectly conducting, semi-infinite leads are linked to a $4\,\mu\text{m} \times 2\,\mu\text{m}$ sample with a disorder potential V_d and a confining potential V_b. $V_d(\boldsymbol{r})$ is a sum of random short-range Gaussians (10–30 nm) generating elastic scattering in the sample, while $V_b(\boldsymbol{r})$ confines the electrons to the sample. We restrict the sample's Hilbert space to the $L_x L_y B/\phi_0 \sim 10^4$ states of the lowest Landau level (LLL), where $L_x L_y$ is the area of the sample, $B \sim 10\,\text{T}$ and $\phi_0 = h/e$ is the magnetic flux quantum. In the guiding-center representation of the LLL, the sample Hamiltonian is a large, sparse matrix [16]. The leads are modeled as ensembles of semi-infinite one-dimensional tight-binding chains attached to LLL states localized on the corresponding edges of the sample [16]. The method of solving the scattering problem described in ref. [16] allows for very general coupling of the leads to the sample, but it is otherwise equivalent to the usual Green's function technique [17]. Further modeling details will be reported elsewhere [18]. For a given magnetic field B, we numerically solve the full scattering problem for different values of the Fermi energy and calculate $\hat{g}(E_F)$.

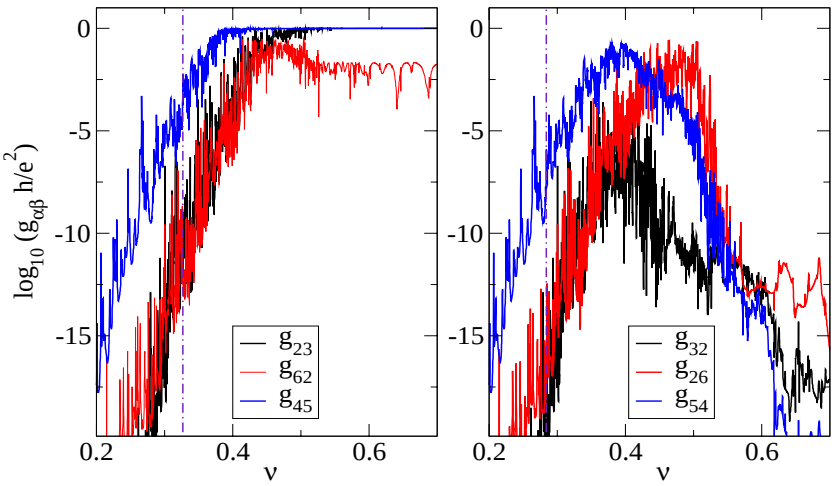

Fig. 2 – (Color online) Representative conductance matrix elements, in units of e^2/h, as a function of the filling factor ν. The left (right) panel shows g_{23}, g_{45} and g_{62}, respectively g_{32}, g_{54} and g_{26}, characterizing transport in the (against the) direction of the edge currents. Results are almost identical on the left of the dot-dashed line, but different on its right.

The filling factor ν is also a function of E_F, and therefore we can find $\hat{g}(\nu)$.

The resistances are then computed from $\hat{g}$. In the usual experimental setup the current is injected in the source and extracted in the drain $-I_1 = I_4 = I$: $\hat{I}_{14} = (-I, 0, 0, I, 0, 0)^T$. Without loss of generality we set $I = 1$ and $V_4 = 0$. The other five contact voltages are uniquely determined from $\hat{I}_{14} = \hat{g} \cdot \hat{V}$. We define two longitudinal resistances $R^L_{14,23} = (V_2 - V_3)/I = V_2 - V_3$, $R^L_{14,65} = V_6 - V_5$, and two Hall resistances $R^H_{14,62} = V_6 - V_2$, $R^H_{14,53} = V_5 - V_3$.

In fig. 2, we plot representative matrix elements $g_{\alpha\beta}$ as a function of ν. For $\nu > 0.5$, $g_{\alpha,\alpha+1} \to e^2/h$ (if $\alpha = 6$, $\alpha + 1 = 1$), with all other off-diagonal matrix elements vanishing. In other words, all electrons leaving contact $\alpha + 1$ scatter into contact α, and therefore [17]

$$g(\nu) \overset{\nu\to 1}{\longrightarrow} g^{(0)} = \frac{e^2}{h} \begin{pmatrix} -1 & 1 & 0 & 0 & 0 & 0 \\ 0 & -1 & 1 & 0 & 0 & 0 \\ 0 & 0 & -1 & 1 & 0 & 0 \\ 0 & 0 & 0 & -1 & 1 & 0 \\ 0 & 0 & 0 & 0 & -1 & 1 \\ 1 & 0 & 0 & 0 & 0 & -1 \end{pmatrix}. \tag{1}$$

Solving $\hat{I}_{14} = \hat{g}^{(0)} \cdot \hat{V}$, we find $V_5 = V_6 = h/e^2$, $V_2 = V_3 = 0$, thus $R^H_{14,62} = R^H_{14,53} = h/e^2$, $R^L_{14,23} = R^L_{14,65} = 0$. This shows that the first quantized plateau is due to the chiral edge currents (shown as oriented thick lines in fig. 1(b)), which become established for $\nu > 0.5$. Variations of $\hat{g}(\nu)$ from $\hat{g}^{(0)}$ give rise to fluctuations in the resistances. From fig. 2 we also see that if $\nu < \nu_c$ (vertical line), $g_{\alpha\beta} \approx g_{\beta\alpha}$ with high accuracy, *i.e.* $\hat{g}$ is symmetric. For $\nu > \nu_c$, $\hat{g}$ is not symmetric. The reasons for this behavior and its consequences are discussed later.

Solving $\hat{I}_{14} = \hat{g}(\nu) \cdot \hat{V}$ for $\hat{g}(\nu)$ shown in fig. 2, we find the various resistances as a function of $0 < \nu < 1$. Figure 3(a) shows a pair R_L and R_H. Three different regimes appear: for $\nu > 0.46$, $R_H = h/e^2$ and $R_L = 0$, corresponding to the first IQHE plateau. For $0.42 < \nu < 0.46$, R_L exhibits large fluctuations while R_H is quantized. This is precisely the type of behavior observed in ref. [1]. For $\nu < 0.42$, the transition to the insulating phase occurs, and both

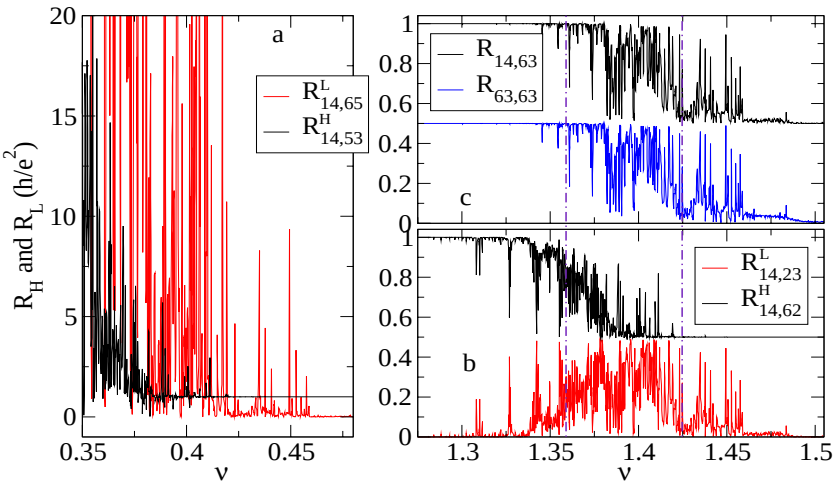

Fig. 3 – (Color online) R_L and R_H calculated from the conductance matrix displayed in fig. 2, in units of h/e^2. (a) Transition from the insulator to the first IQHE plateau in the LLL. (b) Transition from the first to the second IQHE plateaus. (c) The sum $R_L + R_H = R_{14,63}$ of the resistances shown in (b), and $R_{2t} = R_{63,563}$ (displaced by $-0.5h/e^2$). Vertical lines separate the various fluctuation regimes.

resistances increase sharply. The fluctuations are very large and sharp because the calculation is done at $T = 0$. At finite T, the peaks are smeared out.

The transition $1 < \nu < 2$ can also be investigated using the same $\hat{g}(\nu)$ matrix of the LLL. Similar to ref. [19], we assume that the completely filled spin-up LLL contributes its background chiral edge current. As a result, we simply add $\hat{g}^{(0)} = \hat{g}(\nu = 1)$ of eq. (1) to the values of $\hat{g}(\nu)$ describing the partially filled spin-down LLL. Although the two LLLs have different spins, the contacts mix electrons with both spins in equilibrium, justifying this addition. Resistances $R^H_{14,62}$ and $R^L_{14,23}$ computed from $\hat{g}^{(0)} + \hat{g}(\nu)$ are shown in panel (b) of fig. 3, whereas in panel (c) we plot their sum $R^L_{14,23} + R^H_{14,62} = R_{14,63}$. The three regimes found experimentally [2, 3] are clearly observed. At low-ν (high-B), the fluctuations of R_H and R_L are correlated, $R_L + R_H = h/e^2$. At high-ν (low-B) $R_H = h/2e^2$ is quantized while R_L still exhibits strong fluctuations. In the intermediate regime, both R_H and R_L have strong, uncorrelated fluctuations. The other pair, $R^H_{14,53}$ and $R^L_{14,65}$, also exhibits these three regimes, although their detailed fluctuations are different from $R^H_{14,62}$ and $R^L_{14,23}$. From over 20 different simulations we found that the low-ν regime where $R_L + R_H = h/e^2$ is a very robust feature, although it is maintained up to different values of ν in different samples. The high-ν regime with fluctuations in R_L and quantized R_H is seen frequently. However, when strong direct tunneling occurs between the source or the drain and their nearby voltage probes, R_H also fluctuates. Such strong tunneling is an artifact of our simulation [20]. We suppress it by isolating the source and drain from nearby contacts with triangular potential barriers in the corners of the sample (see fig. 1(a)). Figure 3(c) also compares $R^L + R^H = R_{14,63}$ with $R_{2t} = R_{63,63}$. (In the setup for measuring R_{2t}, the current is $\hat{I}_{63} = (0, 0, 1, 0, 0, -1)^T$, and $R_{2t} = V_6 - V_3$.) As found experimentally [2], the two curves are very similar.

So far, we have demonstrated that our numerical simulations reproduce the experimental results. We now explain the underlying physics using a simple but very general model. We introduce the 6×6 matrix $\hat{l}(a,b)|_{\alpha\beta} = \frac{e^2}{h}(\delta_{\alpha a}\delta_{\beta b} - \frac{1}{2}\delta_{\alpha a}\delta_{\beta a} - \frac{1}{2}\delta_{\alpha b}\delta_{\beta b})$. Let $\hat{r}(a,b) = \hat{l}(a,b) + \hat{l}(b,a)$. Solving $\hat{I} = \hat{r}(a,b) \cdot \hat{V}$ shows that $\hat{r}(a,b)$ describes a h/e^2 resistor between contacts a

and b. Since $\hat{r}(a,b)$ is symmetric, the symmetric part $\hat{g}_s$ of the conductance matrix $\hat{g}$ is $\hat{g}_s = \sum_{a<b} r_{ab}\hat{r}(a,b)$, where $r_{ab} = \min(p_{a\to b}, p_{b\to a})$. Given the constraints on $\hat{g}$, we find [18] that the remaining terms group into $\hat{g} - \hat{g}_s = \sum_{a_1\neq\cdots\neq a_n} c_{a_1,\ldots a_n}\hat{r}(a_1,\ldots,a_n)$. Here, $a_1 \to a_2 \to \cdots \to a_1$ is a closed chiral loop linking $3 \le n \le 6$ of the contacts, with a direction of flow dictated by the sign of B. The c's are positive numbers, and $\hat{r}(a_1,\ldots,a_n) = \hat{l}(a_1,a_2) + \cdots + \hat{l}(a_n,a_1)$. For example, $\hat{r}(1,2,3,4,5,6) = \hat{g}^{(0)}$ of eq. (1) describes the edge currents of the full LL, but shorter chiral currents ($n < 6$) may also contribute to $\hat{g}(\nu)$ at intermediate ν.

At low-ν, all states are localized and transport in the LL can only occur through tunneling. The semi-classical limit of a possible scattering scenario is sketched on the left side of fig. 1(c). Electrons can go from 2 to 1 either through direct tunneling (with amplitude t_{21}), or by tunneling to a localized state near contact 6, and from there back to 1, with amplitude $r_{21}t_{26}t_{61}r_{12}e^{i\varphi}$ [21]. Here φ is the phase shift from propagating on chiral states near the three contacts. Electrons can make any number of such loops before entering 1; summing over all we find the total scattering probability to be $p_{2\to1} = |t_{21} + r_{21}t_{26}t_{61}r_{12}e^{i\varphi}/(1 - t_{26}t_{61}t_{12}e^{i\varphi})|^2 \approx |t_{12}|^2 + 2\,\mathrm{Re}(t_{12}t_{26}t_{61}e^{i\varphi}) + \mathrm{O}(t^4)$. Similar arguments give $p_{1\to2} = |t_{12}|^2(1 - |t_{16}|^2)(1-|t_{26}|^2)/|1-t_{26}t_{61}t_{12}e^{i\varphi}|^2 \approx |t_{12}|^2+\mathrm{O}(t^4)$. Thus $g_{12} \approx g_{21}$ and their main contribution to $\hat{g}$ is $|t_{12}|^2\hat{r}(1,2)$. The non-symmetric part $c = 2\,\mathrm{Re}(t_{12}t_{26}t_{61}e^{i\varphi})$ contributes to a small chiral current between contacts 1, 2, 6, as can be checked by computing g_{16}, g_{61}, g_{26} and g_{62} similarly. These processes contribute a total of $r_{12}\hat{r}(1,2) + r_{16}\hat{r}(1,6) + r_{26}\hat{r}(2,6) + c\hat{r}(1,2,6)$ to $\hat{g}$. The symmetric resistance terms, of order $|t|^2$, are due to direct tunneling between contacts, and at low-ν they dominate the small chiral currents, of order $|t|^3$. This explains why for $\nu < \nu_c$, $\hat{g}$ is symmetric to high accuracy (see fig. 2). At higher ν, edge states connecting consecutive contacts appear. As already discussed, as $\nu \to 1$, $\hat{g} \to \hat{g}^{(0)}$. For intermediate ν, shorter chiral loops containing edge states can be established through tunneling, as sketched on the right side of fig. 1(c). Assume that an electron leaving contact 3 can tunnel with amplitudes t_3 and t_5 to and out of a localized state, to join the opposite edge current and enter 5. It follows [10] that $p_{3\to5} = \frac{h}{e^2}g_{53} = |t_3t_5/[1 - r_3r_5\exp[i2\pi\phi/\phi_0]]|^2$, while $p_{5\to3} = 0$ (no electron leaving 5 enters 3). Here ϕ is the flux enclosed in the localized state. Then $r_{35} = \min(p_{3\to5}, p_{5\to3}) = 0$ and the contribution to $\hat{g}$ is just $p_{3\to5}\hat{l}(5,3)$. This term combines with parts of $\hat{l}(3,4)$ and $\hat{l}(4,5)$ to create a chiral current $p_{3\to5}\hat{r}(3,4,5)$. Physically, this contribution describes the back-scattered current of the Jain-Kivelson model [10].

In general, the transport involves both tunneling and chiral currents, but $\hat{g}$ can always be decomposed into symmetric resistances terms plus chiral loops. Consider the general form

$$\begin{aligned}\hat{g} \;=\; & n\hat{g}^{(0)} + r_{12}\hat{r}(1,2) + r_{16}\hat{r}(1,6) + r_{26}\hat{r}(2,6) + r_{34}\hat{r}(3,4) + r_{45}\hat{r}(4,5) + r_{35}\hat{r}(3,5) + c_0\hat{g}^{(0)} + \\ & + c_1\hat{r}(1,2,6) + c_2\hat{r}(2,3,5,6) + c_3\hat{r}(3,4,5) + c_4\hat{r}(1,2,3,5,6) + c_5\hat{r}(2,3,4,5,6).\end{aligned}$$

The first term describes the contribution of the n completely filled lower LLs. All other terms describe transport in the LL hosting E_F (see fig. 1(b)), with the restriction that there is no tunneling between the left and the right side of the sample. This is justified physically because tunneling between contacts far apart is negligible. The largest such terms, r_{23} and r_{56}, are found to be less than 10^{-4} (see, *e.g.*, fig. 2, where $r_{23} = h/e^2 \cdot \min(g_{23}, g_{32})$). Solving both $\hat{I}_{14} = \hat{g}\cdot\hat{V}$ and $\hat{I}_{63} = \hat{g}\cdot\hat{V}'$ we find the identity

$$R_{14,63} = R_{63,63} = \frac{h}{e^2}\frac{1}{n + c_0 + c_2 + c_4 + c_5}\,.$$

Since $R_{63,63} = R_{2t}$, whereas $R_{14,63} = R^H_{14,62} + R^L_{14,23} = R^L_{14,65} + R^H_{14,53}$, this means that $R_{2t} = R_H + R_L$ irrespective of the value of the 12 parameters. In other words, this identity is obeyed for all ν, in agreement with fig. 3(c) (the r_{23} and r_{56} terms lead to perturbative

corrections [18]). Here $n + c_0 + c_2 + c_4 + c_5$ is the total chiral current flowing along the $6 \to 5$ and $3 \to 2$ edges. At low ν, where edge states are not yet established, chiral currents in the LL hosting E_F are negligible, $c_0 = c_2 = c_4 = c_5 = 0$ (as discussed, pure tunneling contributions are of order $c \sim |t|^3$. Below ν_c, all $|t|^2 < 10^{-4}$, see fig. 2). It follows that here $R_L + R_H = h/ne^2$, explaining the perfect correlations of the two resistances at low ν, observed both experimentally and numerically.

The high-ν regime with quantized R_H and fluctuating R_L can also be understood easily. As discussed, the transport in the LL hosting E_F is dominated here by the edge states; tunneling between opposite edge states (facilitated by localized states inside the sample) creates back-scattered currents, as in the Jain-Kivelson model [10]. We sketch this situation in fig. 1(d). Let t_1, t_2 and t_3 be total probabilities for all possible tunneling processes leading to back-scattering on the corresponding pairs of edge states. Reading the various scattering probabilities off fig. 1(d), we find that $\hat{g} = n\hat{g}^{(0)} + (1 - t_1 - t_2 - t_3)\hat{g}^{(0)} + t_2[\hat{r}(1,2,6) + \hat{r}(3,4,5)] + t_3\hat{r}(1,2,3,5,6) + t_1\hat{r}(2,3,4,5,6)$. The first term represents the contribution of the lower n completely filled LLs, the others are the forward and the back-scattered chiral currents in the LL hosting E_F. $\hat{I}_{14} = \hat{g} \cdot \hat{V}$ is trivial to solve. We find $R^H_{14,62} = R^H_{14,53} = h/(n+1)e^2$, *i.e.* the Hall resistances are precisely quantized, whereas $R^L_{14,23} = R^L_{14,65} = [h/(n+1)e^2] \cdot t_2/(n+1-t_2)$. Since t_2 has a strong resonant dependence on E_F (or ν), it follows that here the two R_L fluctuate strongly, but have the same pattern, as indeed shown experimentally in ref. [3]. In particular, if $n = 0$ (transition inside spin-up LLL), R_L can be arbitrarily large when $t_2 \to 1$, whereas in higher LLs the amplitude of fluctuations in R_L is $h/[n(n+1)e^2]$ or less, as observed both experimentally and in our simulations.

We have verified that the Onsager relation $\hat{g}(-B) = [\hat{g}(B)]^T$ holds [14]. The reason is that the time-reversal symmetric tunneling is not affected by this sign change, while the flow of the chiral currents is reversed. The model mirrors itself with respect to the horizontal axis if $B \to -B$, see fig. 1. The solutions of $\hat{I}_{14} = \hat{g}(-B) \cdot \hat{v}$ are related to the solutions of $\hat{I}_{14} = \hat{g}(B) \cdot \hat{V}$ by $v_2 = V_6$, $v_3 = V_5$, $v_5 = V_3$ and $v_6 = V_2$, provided that the same index exchanges, $2 \leftrightarrow 6$, $3 \leftrightarrow 5$, are performed for all r_{ab} terms. Terms not invariant under this transformation are r_{12}, r_{16}, r_{43}, r_{45}, r_{23} and r_{56}. As already discussed, the last two terms are vanishingly small. In the experimental setup, the first four terms are also very small, due to the long distance between source and drain, and their nearby contacts [20]. The dominant terms r_{26} and r_{35} are invariant under the index exchange. Hence, it follows that $R^L_{14,23}(B) = R^L_{14,65}(-B)$ and vice versa, *i.e.* with good accuracy, the fluctuation pattern of one R_L mirrors that of the other R_L when $B \to -B$. This symmetry has indeed been observed experimentally, with small violations at low ν [3] due to small corrections from the non-invariant contributions r_{12}–r_{16} and r_{43}–r_{45} [18].

We now summarize our understanding of the various results of IQHE measurements on mesoscopic samples. Similar to experiments, we find that the transition in higher LLs is naturally divided in three regimes. At low ν, the LL hosting E_F is insulating and there are no edge states connecting the left and right sides of the sample. If tunneling between left and right sides is also small, we find that the fluctuations of pairs of resistances are correlated with excellent accuracy, $R_H + R_L = h/ne^2$. This condition is obeyed if the typical size of the wave function (localization length) is less than the distance between contacts 2 and 3. When the size of the wave function becomes comparable to this distance, edge states are established and the correlation between R_L and R_H is lost. On the high-ν side, the edge states are established, but localized states inside the sample can help electrons tunnel between opposite edges, leading to back-scattering as in the Jain-Kivelson model. In this case, we showed that R_L fluctuates while R_H is quantized. Tunneling between opposite edges is likely only

if the typical size of the wave function is slightly shorter than the distance between opposite edges. It is then apparent that the central regime in figs. 3(b) and (c) corresponds to the so-called "critical region", where the typical size of the electron wave function is larger than the sample size (distance between contacts 2 and 3, at low ν, or between 2 and 6 at high ν). In these mesoscopic samples, the voltage probes act as markers on a ruler, measuring the size of the wave functions at the Fermi energy. To our knowledge, this is the first time when the boundaries of the critical region are pinpointed experimentally. This opens up exciting possibilities for experimentally testing the predictions of the localization theory of IQHE.

To conclude, we used both first-principles simulations and a simple model for the general allowed structure of the conductance matrix to explain the phenomenology of the mesoscopic IQHE, for the six-terminal geometry. We identified tunneling and chiral currents as coexisting mechanisms for charge transport in these mesoscopic samples, and argued that the boundaries between the three distinct fluctuation regimes mark the critical region.

* * *

This research was supported by NSERC and NSF DMR-0213706. We thank Y. Chen, E. Peled, R. Fisch, R. N. Bhatt and D. Shahar for helpful discussions.

REFERENCES

[1] Peled E., Shahar D., Chen Y., Sivco D. L. and Cho A. Y., *Phys. Rev. Lett.*, **90** (2003) 246802.
[2] Peled E., Shahar D., Chen Y., Diez E., Sivco D. L. and Cho A. Y., *Phys. Rev. Lett.*, **91** (2003) 236802.
[3] Peled E., Chen Y., Diez E., Tsui D. C., Shahar D., Sivco D. L. and Cho A. Y., *Phys. Rev. B*, **69** (2004) 241305.
[4] Chang A. M., and Cho A. Y., *Solid State Commun.*, **76** (1988) 769.
[5] Timp G., Chang A. M., Mankiewich P., Behringer R., Cunningham J. E., Chang T. Y. and Howard R. E., *Phys. Rev. Lett.*, **59** (1987) 732.
[6] Simmons J. A., Wei H. P., Engel L. W., Tsui D. C. and Shayegan M., *Phys. Rev. Lett.*, **63** (1989) 1731.
[7] Cobden D. H., Barnes C. H. W. and Ford C. J. B., *Phys. Rev. Lett.*, **82** (1999) 4695.
[8] Cho S. and Fisher M. P. A., *Phys. Rev. B*, **55** (1997) 1637.
[9] Streda P., Kucera J. and MacDonald A. H., *Phys. Rev. Lett.*, **59** (1987) 1973.
[10] Jain J. K. and Kivelson S. A., *Phys. Rev. Lett.*, **60** (1988) 1542.
[11] Büttiker M., *Phys. Rev. Lett.*, **62** (1989) 229.
[12] Büttiker M., *Phys. Rev. Lett.*, **57** (1986) 1761.
[13] Büttiker M., *Phys. Rev. B*, **38** (1988) 9375.
[14] Baranger H. U. and Stone A. D., *Phys. Rev. B*, **40** (1989) 8169.
[15] Ando T., *Phys. Rev. B*, **49** (1994) 4679.
[16] Zhou C. and Berciu M., *Phys. Rev. B*, **70** (2004) 165318.
[17] Datta S., *Electronic Transport in Mesoscopic Systems* (Cambridge University Press, Cambridge) 1997.
[18] Zhou C. and Berciu M., unpublished.
[19] Shahar D., Tsui D. C., Shayegan M., Shimshoni E. and Sondhi S. L., *Phys. Rev. Lett.*, **79** (1997) 479.
[20] We use short samples ($\approx 4\,\mu\text{m} \times 2\,\mu\text{m}$) in order to save CPU time by decreasing the number of states in the LLL; experimental devices are much longer ($\approx 24\,\mu\text{m} \times 2\,\mu\text{m}$).
[21] The forward scattering amplitudes are equal $|r_{12}| = |r_{21}| = \sqrt{1 - |t_{12}|^2}$, but they may have different phases.